

**MAGNETIC AND STRUCTURAL PROPERTIES OF CoPt NANOPARTICLES
EMBEDDED IN Ag**

by

Yasaman Barekatin

A thesis submitted to the Faculty of the University of Delaware in partial fulfillment of the requirements for the degree of Master of Science in Physics

Summer 2017

© 2017 Yasaman Barekatin
All Rights Reserved

**MAGNETIC AND STRUCTURAL PROPERTIES OF CoPt NANOPARTICLES
EMBEDDED IN Ag**

by

Yasaman Barekatin

Approved: _____
George C. Hadjipanayis, Ph.D.
Professor in charge of thesis on behalf of the Advisory Committee

Approved: _____
Edmund R. Nowak, Ph.D.
Chair of the Department of Physics and Astronomy

Approved: _____
George Watson, Ph.D.
Dean of the College of Arts and Sciences

Approved: _____
Ann L. Ardis, Ph.D.
Senior Vice Provost for Graduate and Professional Education

ACKNOWLEDGMENTS

I would like to thank everyone who helped me with this accomplishment, especially my adviser, Dr. Hadjipanayis for his support and guidance. I am very grateful to my family for their love, encouragement and endless support. Very especial thanks to my parents for providing me with opportunities to improve and succeed. I am also very grateful to my dear brothers, Armin and Amir, for being always encouraging and supportive.

I also would like to thank Aleksandr Gabay for his invaluable help and advices. I also would like to thank Taha Salavatifard for being a very good officemate and friend. I appreciate Harsha Kannan's help during this work. I also would like to thank all my friends: Shirin Pourmiri, Abhishek Sharan, Hassan Shahfar, Onur Tosun, Frank Abel, Mojtaba Taghipour and Vimal Deepchand,

TABLE OF CONTENTS

LIST OF FIGURES	vi
ABSTRACT.....	ix
Chapter	
1 INTRODUCTION	1
1.1 Origin of Magnetism.....	1
1.2 Magnetic Material's Applications.....	1
1.3 Different Types of Magnetic Materials.....	2
1.3.1 Diamagnetic Materials.....	2
1.3.2 Paramagnetic Materials.....	2
1.3.3 Ferromagnetic Materials.....	3
1.3.4 Antiferromagnetic Materials.....	4
1.3.5 Ferrimagnetic Materials.....	4
1.4 Hysteresis Loop	4
1.5 Domains and Single Domain Particles	5
1.6 Magnetization Behavior of a Single Domain Particles in Presence of a Magnetic Field	7
1.7 Coercivity Dependence on the Grain Size	10
1.8 Cobalt-Platinum.....	12
1.8.1 Phase Diagram of Cobalt-Platinum	12
1.8.2 Applications of Cobalt-Platinum in High Density Recording	15
1.8.3 Previous Studies on Cobalt-Platinum Nanoparticles	16
2 EXPERIMENTAL METHODS.....	18
2.1 Magnetron Sputtering Machine	18
2.1.1 Sample Preparation	18
2.2 Heat Treatment.....	20
2.3 Sample Characterization	20
2.3.1 X-ray Diffraction	20
2.3.2 Vibrating Sample Magnetometer.....	22
2.3.3 Transmission Electron Microscopy	22
3 RESULTS AND DISCUSSIONS.....	23

3.1	CoPt Thin Film	23
3.2	As-deposited and Annealed CoPt/Ag	25
3.2.1	Structural Properties of the As-deposited and Annealed CoPt/Ag	26
3.2.2	Magnetic Properties of As-deposited and Annealed CoPt/Ag	28
3.2.2.1	Hysteresis Loop of CoPt/Ag	28
3.2.2.2	Dependence of Coercivity on Annealing Time	29
3.2.2.3	Coercivity as a Function of Temperature.....	34
3.2.3	Annealing Temperature Effects on the Structure and the Magnetic Properties of CoPt/Ag.....	37
3.2.4	Microstructure of As-deposited and Annealed CoPt/Ag	41
4	CONCLUSION.....	43
	REFERENCES	45

LIST OF FIGURES

Figure 1.1:	This figure shows magnetization and hysteresis loop for a ferromagnetic material. OABC is the magnetization loop, and CEFGC is hysteresis loop. ⁸	5
Figure 1.2:	This figure shows a uniaxial particle, with M_s makes an angle Θ with the easy axis, and a magnetic field makes an angle α with the easy axis. ¹	7
Figure 1.3:	This figure shows reduced magnetization versus reduced field for different angles between a field and the easy axis. ¹	8
Figure 1.4:	This figure shows the energy barrier for different values of a magnetic field. When $h=0$, there is no external field and the energy barrier is symmetric. And when $h=h_c$, energy barrier will be zero and magnetization reversal happens. ¹	9
Figure 1.5:	In this figure, the solid line shows hysteresis behavior of randomly oriented single domain particles, while dashed line shows the hysteresis behavior of single domain particle or an assembly of parallel single domain particles with their c axis parallel to a field. ¹ ..	10
Figure 1.6:	This figure shows the grain size dependence of the coercivity. In the figure, SP means superparamagnetic, S-D means single domain, and M-D represents multi-domain particle. ¹¹	11
Figure 1.7:	Equilibrium phase diagram of cobalt-platinum system. ¹⁴	12
Figure 1.8:	Left figure shows the disordered fcc structure with Co/Fe and Pt particles occupying each site with the same probability. Right figure shows ordered fct, with Co/Fe atoms sitting on the corner and two faces, and Pt atoms sitting on the rest of sites. During ordering c axis shrinks to make c/a less than one. ¹¹	14
Figure 1.9:	Dependence of the lattice parameters of the cobalt-platinum alloy. ¹⁴	14
Figure 2.1:	This schematic shows the sputtering chamber. ¹¹	19
Figure 2.2:	Bragg's diffraction from atoms of crystal. d is the distance between the crystal's plane. ²²	21

Figure 3.1: The XRD pattern of as-deposited, annealed at 900°C, and 700°C CoPt single film. The sharp peak around 33 degrees is from the Si substrate.	24
Figure 3.2: The hysteresis loops for as-deposited and annealed CoPt thin film. The as-deposited CoPt thin film shows very low coercivity, while the annealed CoPt thin film shows very high coercivity.	25
Figure 3.3: XRD patterns of the [(CoPt)5nm/(Ag)t]n multilayer samples. The peak at 33° is from substrate. Silver has peaks at 38° and 44°.....	27
Figure 3.4: This figure shows the integrated intensities ratio of $I_{(001)}/I_{(111)}$ for annealed [(CoPt)5nm/(Ag)t]n sample with t= 0, 2, 5 and 10 nm. Annealing was done at 700°C for 60 min.....	28
Figure 3.5: This figure shows the hysteresis loops for the as-deposited and the annealed [(CoPt)5nm/(Ag)t]n samples with t= 0.6, 2, 5 and 10 nm ..	29
Figure 3.6: Coercivity versus annealing time. Annealing was done at 700°C.....	30
Figure 3.7: This figure shows the lattice parameters and the c/a for the samples annealed at 700°C. a and c were found from d spacing of (200) and (002) peaks, respectively.	32
Figure 3.8: This figure compares the coercivity with the silver layer thickness for two different annealing times.	34
Figure 3.9: This figure shows the hysteresis loops for the (5/10) nm*10 sample annealed for 1h at 700°C. Coercivity increased when measurement done in lower temperature.	36
Figure 3.10: Coercivity as a function of temperature for the (5/10) nm*10 sample annealed at 700C for 1h.....	36
Figure 3.11: XRD patterns for the (5/10) nm and (5/2) nm samples annealed at 600°C, 700°C and 750°C for 60 min.....	37
Figure 3.12: This figure shows c/a found from (002) and (200) peaks for (5/10) nm*10 and (5/2) nm*21 samples annealed for 60 min at three different temperature.....	38
Figure 3.13: Hysteresis loops for (5/10) *10 and (5/2) *21 samples annealed for 60min at different temperatures.....	40

Figure 3.14: H_c versus annealing temperature. 41

Figure 3.15: (a) As-deposited (5/2) nm. SAD pattern shows fcc structure for CoPt and Ag. (b) (5/10) nm annealed at 700°C for 15min. The average particle size is 79.7nm \pm 25nm. (c) (5/10) nm annealed at 700°C for 60min with average particle size of 93nm \pm 23nm. (d) (5/10) nm annealed at 700°C for 120min. The average particle size is 87nm \pm 42nm. (e) (5/2) nm annealed at 700°C for 15min with average particle size of 51nm \pm 22nm. (f) (5/2) nm annealed at 700°C for 60min with average particle size of 26nm \pm 14nm. (g) (5/.6) nm annealed at 700°C for 15min with average particle size of 28nm \pm 22nm. (h) (5/.6) nm annealed at 700°C for 120min with average particle size of 27nm \pm 11nm. 42

ABSTRACT

$L1_0$ CoPt nanoparticles have very high magnetocrystalline energy that makes them potential candidate for high density recording media. In this study, I have investigated the structural and magnetic properties of CoPt particles embedded in silver. The CoPt nanoparticles were produced from CoPt/Ag multilayers. The thickness of CoPt layer was kept the same, and the thickness of Ag layer was varied. The as-made samples had the fcc structure. Particles with the ordered $L1_0$ structure were obtained by annealing the multilayers at a high temperature. The highest coercivity and particle size were found in samples with larger Ag layer thickness. Also, samples with larger Ag layer thickness showed the ordering in lower annealing time and temperature. Samples with smaller Ag layer thickness shows larger degree of ordering in comparison with the ones with larger Ag layer thickness.

Chapter 1

INTRODUCTION

1.1 Origin of Magnetism

To understand the magnetic behavior of any material, we need to study the magnetic moment of each atom. The total magnetic moment of an atom is

$$\mathbf{m}_{atom} = -g_{atom} \frac{e}{2m_e} \mathbf{J} \quad (1.1)$$

Where g_{atom} is spectroscopic factor, m_e is mass of the electron, e is electron charge and \mathbf{J} is the total angular momentum vector which is the sum of the spin angular momentum, \mathbf{S} , and orbital angular momentum, \mathbf{L} .

$$\mathbf{J} = \mathbf{S} + \mathbf{L} \quad (1.2)$$

The magnitude of the total magnetic moment of an atom comes from below equation

$$|\mathbf{m}_{atom}| = g_{atom} \frac{eh}{2m_e\pi} \sqrt{J(J+1)} = g_{atom} \mu_B \sqrt{J(J+1)} \quad (1.3)$$

Where μ_B is Bohr magnetron. Depends on the value of J , atom can have zero or non-zero magnetic moment, and shows different magnetic behavior. ¹

1.2 Magnetic Material's Applications

Magnetic materials are having the broad applications. Magnetic nanoparticles are used in medicine as a drug delivery, MRI contrast agents and to introduce hyperthermia as a possible treatment for cancer. They are also used as catalysts.² Another important application of magnetic material is in magnetic recording industry. Writing head, reading head, and recording media are made of magnetic materials.³

Some common materials which are used in density recording media are cobalt-based alloys with hexagonal structure. However, magnetic alloys with $L1_0$ structure like CoPt and FePt and rare earth transition metals like Co_5Sm are having much higher, magnetocrystalline anisotropy, K_u , and are more desirable for high density recording media. ^{4,5}

Hard magnetic materials with coercivity equal and greater than 400 kA/m are used as refrigerator magnets, sensors, dc motors or generators, wind mills, and holding devices, etc. Soft magnetic materials with coercivity of 10 kA/m or less is useful for microwave applications, electrical steels and transformers, etc. ⁶

1.3 Different Types of Magnetic Materials

1.3.1 Diamagnetic Materials

In these materials, since the atomic levels are full, J is zero, and there is no net atomic magnetic moment. When these materials are placed in an external magnetic field, they are repelled by it. It happens because an external magnetic field induces a magnetic moment which is in the opposite direction of a magnetic field. These materials have a very small and negative susceptibility. Diamagnetism is the properties of the all the materials. But it is significant when a material does not show any other magnetic behaviors. ¹

1.3.2 Paramagnetic Materials

In contrast with the diamagnetic materials, atoms in paramagnetic materials are having nonzero magnetic moment. These magnetic moments are randomly distributed, and result in zero net magnetization. These materials are having small and positive susceptibility, follows by Curie law.

$$\chi = \frac{C}{T} \quad (1.4)$$

When these materials are placed on an external magnetic field, their magnetic moments start to align themselves to the direction of a magnetic field, and they show a non-zero net magnetization. When a magnetic field is removed, a material shows a zero magnetization.^{1,6}

1.3.3 Ferromagnetic Materials

Ferromagnetic materials are another type of the magnetic materials. Iron, nickel, cobalt and their alloys belong to this group. In these materials, each atom has nonzero magnetic moment and there is an exchange interaction between them, which results in spontaneous parallel alignment of the magnetic moments inside each domain. Therefore, in an absence of an external field, each domain has nonzero spontaneous magnetization. In multi-domain ferromagnetic materials, domains are aligned in a way that net magnetization will be zero without an external field. Sufficiently large field can align all the magnetic moments in the direction of a magnetic field. Despite the paramagnetic materials when field is removed, ferromagnetic material can show a nonzero magnetization which depends on the highest value of a field it experienced.

These materials show the ferromagnetic behavior when their temperature is below the critical temperature, T_c . Below critical temperature, they behave like a paramagnetic material. These materials are having a large positive susceptibility that obeys a Curie-Weiss law at a temperature larger than T_c .¹

$$\chi = \frac{c}{T-T_c} \quad (1.5)$$

1.3.4 Antiferromagnetic Materials

In these materials, although each atom has nonzero magnetic moment, neighboring magnetic moments have the same magnitude and are antiparallel due to an exchange interaction between nearest and next nearest neighbors. Therefore, in an absence of a magnetic field there is no net magnetization in these materials. Like, paramagnetic materials, they are having small positive susceptibility. Below Neel temperature, T_N , their susceptibility depends on the direction of an applied field, while above T_N , they show paramagnetic behavior. ¹

1.3.5 Ferrimagnetic Materials

Their behavior is like the ferromagnetic materials. They are having large positive susceptibility. Due to an exchange interaction, magnetic moments are parallel in each sub lattice. But, they are antiparallel with the next sub lattice. Since, magnetic moments in each sub lattice are having different magnitude, there is the net magnetization. ¹

1.4 Hysteresis Loop

Ferromagnetic materials show the hysteresis behavior. In this loop, M_r is called remanence magnetization which is magnetization that material shows after an external field is removed. Coercivity or coercive field, H_c , is the field required to demagnetized the sample after it is magnetized. Magnetization at point C is saturation magnetization, M_s , and it happens when all the magnetic moments are along the magnetic field's direction. The squareness of any hysteresis graph is defined by M_r/M_s , and it can be

and the boundary between each domain is called domain wall. Domains are created in a ferromagnetic material to reduce demagnetization inside a material. In the absence of a magnetic field, domains are oriented in such a way that the net magnetization of a bulk material is zero. Within each domain wall, the magnetic moments are rotating either in plane or out of plane. Domain wall thickness is determined by the competition of two energies: exchange energy which likes to make domain wall as thick as possible, and anisotropy energy which likes to make the wall as thin as possible. Domain wall thickness and energy can be obtained by minimizing sum of these two energies.

$$\delta_{\text{wall}} = \pi\sqrt{A/K_u} \quad (1.6)$$

$$\gamma_{\text{wall}} = 2\pi\sqrt{AK_u} \quad (1.7)$$

where $A = JS^2/a$. Here δ_{wall} is a wall thickness, γ_{wall} is a wall energy and it is minimum when an anisotropy energy and an exchange energy are equaled together. A is called exchange spring constant, and J is exchange integral.

While by adding more domain walls to each grain, demagnetization energy is reduced, at the same time a new domain wall energy is added to the system. We are having single domain particles when the domain wall energy and demagnetization energy become comparable. Therefore, below this size, the particle can have only one domain and there is no domain wall. This particle is called a single domain particle.

For uniaxial material, this size can be obtained with following equation: ⁹

$$D_{SD} = \frac{1.4\gamma_{\text{wall}}}{M_s^2} \quad (1.8)$$

1.6 Magnetization Behavior of a Single Domain Particles in Presence of a Magnetic Field

The magnetization of the single domain particles is based on coherent rotation, and can be described with Stoner-Wohlfarth model.¹⁰ In the absence of an external magnetic field, spontaneous magnetization, M_s , is directed in the direction of the easy axis. When an external field is applied, M_s starts to rotate itself to be aligned with a magnetic field. For a uniaxial single domain particle shown in the figure 1.2, magnetocrystalline energy is equaled to

$$E_k = K_u \sin^2 \theta \quad (1.9)$$

And since the particle is placed under a magnetic field, H , it has Zeeman energy equals to

$$E_h = -\mu_0 H M_s \cos(\alpha - \theta) \quad (1.10)$$

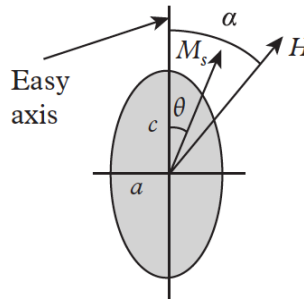


Figure 1.2: This figure shows a uniaxial particle, with M_s makes an angle θ with the easy axis, and a magnetic field makes an angle α with the easy axis.¹

And the total energy of this particle is the sum of these two energies.

$$E_t = K_u \sin^2 \theta - \mu_0 H M_s \cos(\alpha - \theta) \quad (1.11)$$

Here, Zeeman energy wants to orientate M_s along a magnetic field, and magnetocrystalline energy wants to keep M_s along the easy axis. At equilibrium, this total energy should be minimum, so $\partial E_t/\partial\theta=0$, and we have

$$\sin \theta \cos \theta - \frac{\mu_0 H M_s}{K_u} \sin(\alpha-\theta) = 0 \quad (1.12)$$

By defining the reduced field, $h=H/H_k$, where H_k is anisotropy field, we can rewrite (1.12) equation

$$\sin \theta \cos \theta - h \sin(\alpha-\theta) = 0 \quad (1.13)$$

Reduced magnetization is defined by $m=M/M_s$, where M is the magnetization and is equaled to $M=M_s \cos(\alpha-\theta)$. Equation (1.13) shows that depending on the direction and the strength of a magnetic field, different hysteresis loop can be obtained. Figure 1.3 shows different loops for different angles between a magnetic field and the easy axis.

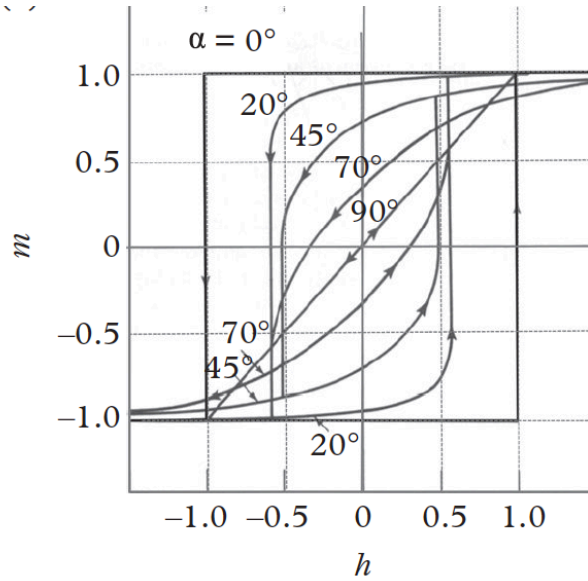


Figure 1.3: This figure shows reduced magnetization versus reduced field for different angles between a field and the easy axis. ¹

When an external field is perpendicular to a magnetic field, $m=h$ and there is no coercivity. If a field and an easy axis have the same direction, a square shaped hysteresis occurs. Here, there is no torque from a magnetic field to rotate the magnetization. Magnetization rotation happens at the coercive field. At this field, the energy barrier between up and down magnetization becomes zero, and magnetization can reverse itself. In this case magnetization switches its direction suddenly, while for other angles, magnetization rotates gradually. Figure 1.4 shows the energy barrier for magnetization reversal at different applied field. ^{1,7}

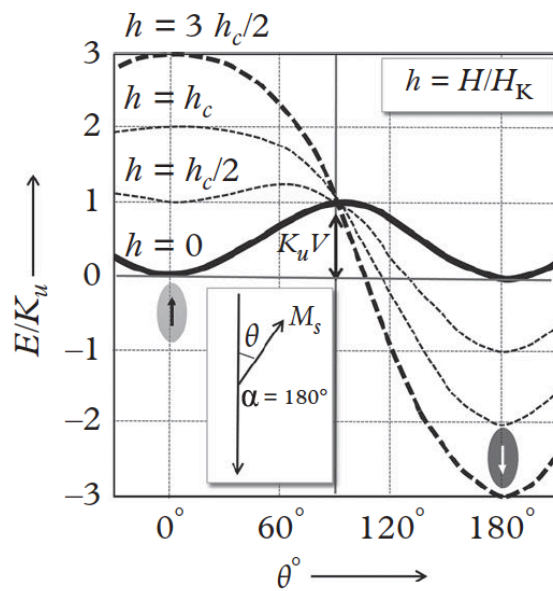


Figure 1.4: This figure shows the energy barrier for different values of a magnetic field. When $h=0$, there is no external field and the energy barrier is symmetric. And when $h=h_c$, energy barrier will be zero and magnetization reversal happens. ¹

If instead of one single domain particle or assembly of parallel single domain particles, there is an assembly of randomly oriented particles, hysteresis loop has the shape of figure 1.5. In this case, coercivity will be equal to $.96K_1/M_s$. And for the randomly oriented spherical particles with cubic crystalline anisotropy, coercivity is equal to $H_c = .64K_1/M_s$.⁸

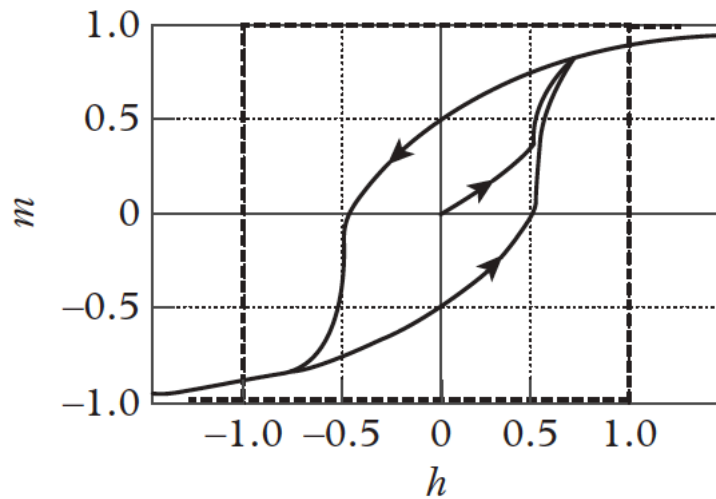


Figure 1.5: In this figure, the solid line shows hysteresis behavior of randomly oriented single domain particles, while dashed line shows the hysteresis behavior of single domain particle or an assembly of parallel single domain particles with their c axis parallel to a field.¹

1.7 Coercivity Dependence on the Grain Size

Size of the particle is one of the factor that coercivity depends on it. Below figure shows the grain size dependence of the coercivity. In this figure, SP means superparamagnetic, S-D means single domain, and M-D represents multi-domain particles. When the size of the particle is below D_p , particle is in superparamagnetic

region and its hysteresis shows no coercivity. By increasing the size of the grain, coercivity increases until it reaches its maximum value. After that by increasing the grain size, coercivity decreases. Coercivity has its maximum value when the grain has the maximum possible size for a single domain particle.

Below equation shows the coercivity as a function of particle size, for field applied parallel to the anisotropy axis.

$$H_c = H_k \left\{ 1 - \left(\frac{V_p}{V} \right)^{\frac{1}{2}} \right\} = H_k \left\{ 1 - \left(\frac{D_p}{D} \right)^{\frac{3}{2}} \right\} \quad (1.14)$$

Where V_p and D_p are critical volume and size for superparamagnetism.^{1 6}

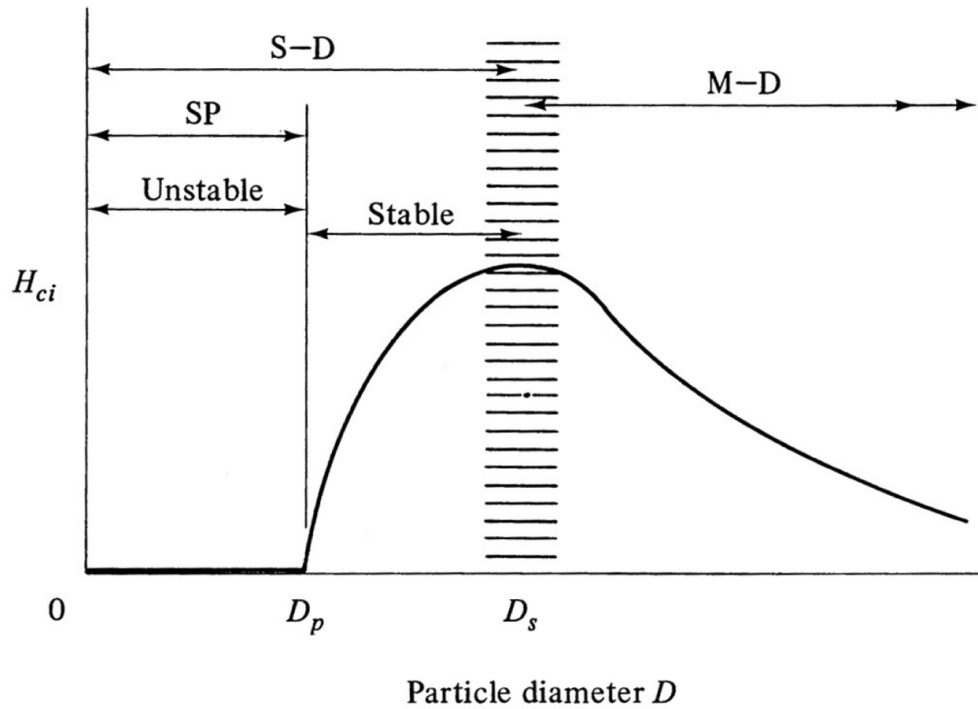


Figure 1.6: This figure shows the grain size dependence of the coercivity. In the figure, SP means superparamagnetic, S-D means single domain, and M-D represents multi-domain particle.¹¹

1.8 Cobalt-Platinum

CoPt has a $L1_0$ structure that makes it suitable candidate for ultra-high density recording. $L1_0$ structures are having very high magnetocrystalline anisotropy energy which makes them more thermally stable.⁵ As a result of high magnetocrystalline energy, they show high coercivity.¹² Also, cobalt-platinum alloys have a high corrosion resistance.¹³

1.8.1 Phase Diagram of Cobalt-Platinum

Figure 1.7 shows the phase diagram of the cobalt-platinum system at equilibrium.

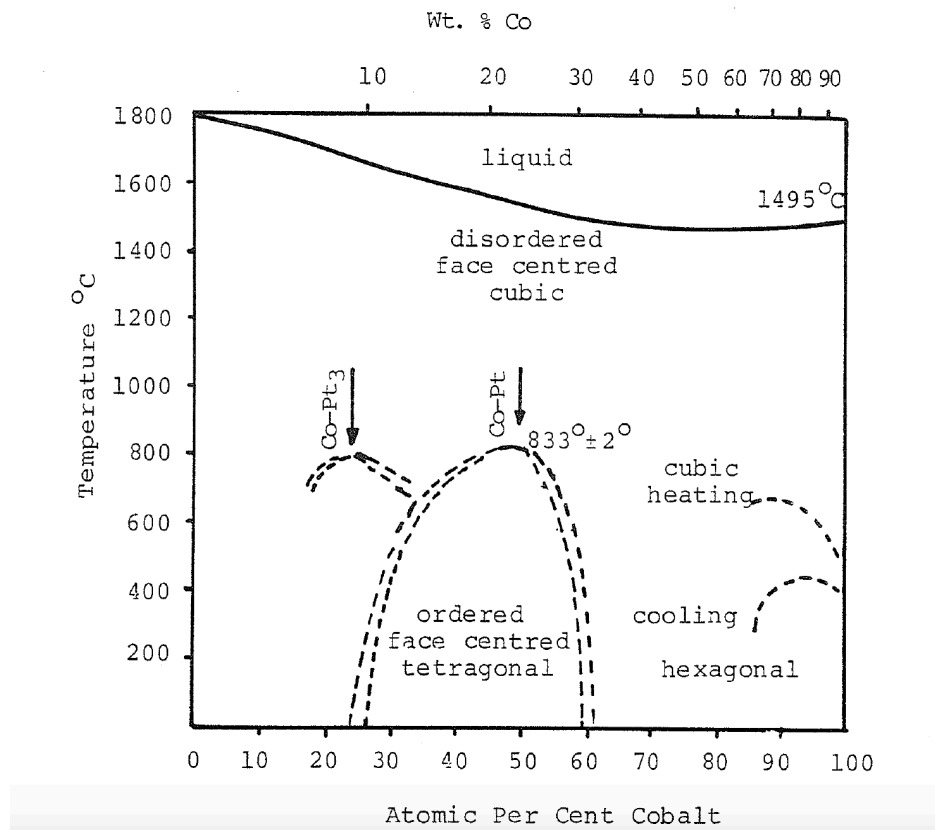


Figure 1.7: Equilibrium phase diagram of cobalt-platinum system.¹⁴

Based on the phase diagram, CoPt with the composition near 50-50% can have either disordered face centered cubic, fcc, or ordered face centered tetragonal, fct, structure. In CoPt, $L1_0$ phase is formed by transition from high temperature disorder fcc phase. $L1_0$ phase in CoPt is stable below the critical temperature which based on the phase diagram is 833°C .⁵ Besides CoPt superstructure, CoPt_3 is also a stable superstructure.¹⁴ Below its critical temperature CoPt_3 has a structure of ordered fcc with the cobalt atoms sitting on the corners and platinum atoms sitting on the faces.¹⁴

FePt has a similar phase diagram. $L1_0$ FePt below the critical temperature which is 1300°C is stable, and above this critical temperature it is disordered fcc.⁵

In general, for fcc alloys, the probability of each atom of each kind occupy each site is the same.⁵ Fcc structures usually show low coercivity, and are magnetically soft. For $L1_0$ structure, the probability of each atom of each kind to occupy each site is not the same. In this case, one kind of the atom is occupying the corners and two faces, and another kind of the atom is occupying the rest of the faces. Therefore, the symmetry of the structure decreased. In $L1_0$ structure, c/a is usually less than 1. Based on the phase diagram, $L1_0$ structure is low temperature phase, and is having lower entropy. For $L1_0$ structure, magnetization vector is usually along the c axis or $[001]$, while the easy axis for fcc CoPt is $[111]$.⁵ For fully ordered CoPt and FePt c/a is equaled to 0.973 and 0.964.¹⁵ Below figures show the cell structure for disordered fcc and ordered fct.

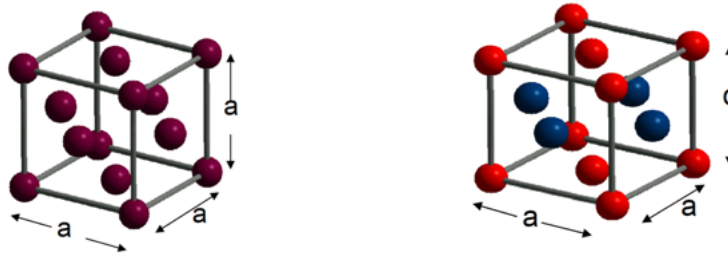


Figure 1.8: Left figure shows the disordered fcc structure with Co/Fe and Pt particles occupying each site with the same probability. Right figure shows ordered fct, with Co/Fe atoms sitting on the corner and two faces, and Pt atoms sitting on the rest of sites. During ordering c axis shrinks to make c/a less than one.¹¹

The dependence of the lattice parameters of the bulk cobalt-platinum alloy can be obtained from the below graph. Based on this graph, cobalt-platinum with the composition of 50-50% has a lattice parameter equals to 3.78 Å.¹⁴

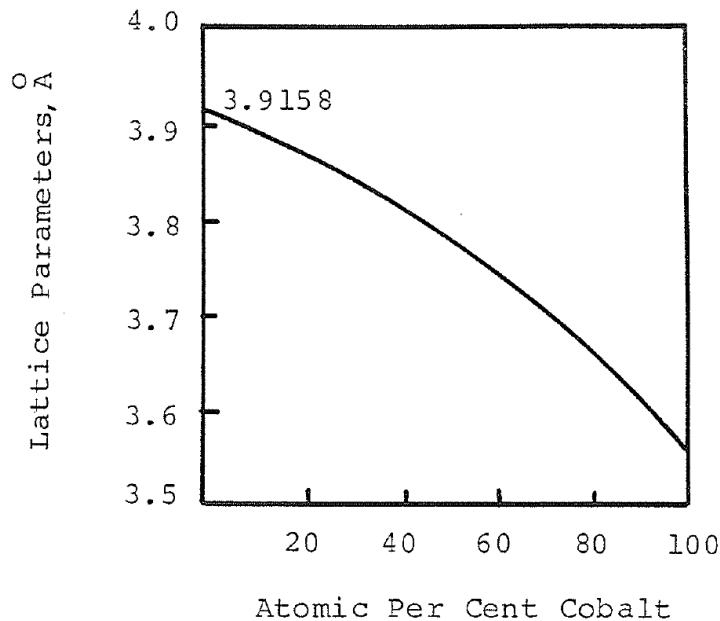


Figure 1.9: Dependence of the lattice parameters of the cobalt-platinum alloy.¹⁴

Also it has been shown that the fully ordered CoPt shows higher coercivity in comparison with mixed ordered and disordered phase.¹³

1.8.2 Applications of Cobalt-Platinum in High Density Recording

In high density recording media, to increase an areal density, the grains size must be decreased. Decreasing the grains size results in thermal instability. It means that in operating temperature, thermal energy can compete with magnetic energy of each grain, and magnetic moments can change their directions. So, in order to use small grains and solve thermal instability problem, we need to use materials with high magnetocrystalline anisotropy energy.³

L1₀ CoPt and FePt with their easy axis along [001] have very high magnetocrystalline anisotropy energies which are around 4.9*10⁷ erg/cm³ and 7*10⁷ erg/cm³ respectively¹⁶, in comparison with disordered fcc CoPt and FePt that have anisotropy constants equal to -6*10⁵ erg/cm³ and 10⁴ erg/cm³¹⁷. Their curie temperature are 840K and 750K for L1₀ CoPt and L1₀ FePt⁴. Therefore, L1₀ CoPt and FePt can be very good candidates for ultra-high density recording media. Because of their importance in high density recording media, controlling the size distribution, particle size and coercivity in L1₀ CoPt and FePt are very important. In high density recording, besides using particles with high anisotropy constants, it is important to increase the signal to noise ratio in media. One way to do this is to fabricate isolated particles to decrease the interaction between particles.^{16 18}

Based on the below equation to satisfy the ten-year relaxation time for grains which is required in high density recording media, L1₀ CoPt and FePt nanoparticles should have minimum size of 4nm and 2.6-3.2 nm respectively.^{16 4}

$$\tau = f_0^{-1} \exp(-E_B/kT) = f_0^{-1} \exp(-K_u V/kT) \quad (1.16)$$

Here in this formula, f_0 is attempt frequency which is around 10^9 for cobalt alloys. k is Boltzmann constant and T is operating temperature. E_B is the energy barrier between two up and down magnetization. V is volume of each grain and K_u is uniaxial anisotropy constant. ¹⁹

1.8.3 Previous Studies on Cobalt-Platinum Nanoparticles

Because of the importance and promising future of CoPt and FePt nanoparticles in high density recording, different studies have been done on them. To fabricate CoPt and FePt nanoparticles that have desirable size and magnetic properties, and narrow size distribution, different methods can be used.

One common way to fabricate CoPt and FePt nanocomposites is to use sputtering. In this method, either multilayers of CoPt or FePt and another material is sputtered on the substrate or CoPt and another material are co-sputtered at the same time. Then by annealing at proper temperature, $L1_0$ CoPt and FePt nanoparticles are fabricated. Different materials can be used as a matrix. For example for FePt, by using C and BN, FePt nanoparticles with size ranging from 3-20nm and H_c ranging from 2 to 16kOe was fabricating. ²⁰

Also, same studies have been done on CoPt/C. Using C as a matrix results in fabrication of CoPt nanoparticles with average size of 7-20nm and coercivity between 3-12kOe. This study shows increasing C concentration decreases the particle size and coercivity. Carbon also can be used to reduce interaction between grains, which results in less media noise and it is very important factor in high density recording. ^{16 10}

Using Ag in CoPt results in ordering happens in lower temperature and enhance (001) orientation in CoPt. ¹² Also, fct CoPt in Ag matrix was fabricated with

CoPt nanoparticles with size and coercivity ranging from 7-100nm and 1-17kOe respectively.⁹

Besides sputtering, different synthesis methods can also be used to fabricate CoPt nanoparticles.

Chapter 2

EXPERIMENTAL METHODS

The focus of this chapter is on the methods used to prepare and characterize the samples.

2.1 Magnetron Sputtering Machine

Magnetron sputtering was used to prepare samples. During the sputtering, positively argon ions with sufficient energy hit the target (cathode), and eject target's atoms. These ejected atoms then move toward the substrate. Large magnet is placed under the target to create magnetic field to confine secondary electrons that are created when Ar ions hit the target. Confining these electrons near cathode increases the chance of ionization of Ar atoms, and subsequently, it results in system to operate in lower voltage.

High deposition rate, high quality film, easy use for metals and their alloys, etc. are some of the advantages to use magnetron sputtering.²¹

2.1.1 Sample Preparation

Sample were prepared by sputtering targets on the Si wafer with (100) orientation coated with one micron SiO₂, and TEM grids coated with carbon. Targets which used here are CoPt alloyed target with four Cobalt chips on its surface to get desirable composition and silver. To making sure composition and thickness uniformity on the sample, the size of the sample prepared is less than 30% of the size of the target. Mask were used to control the area of the sample to be coated.

The below figure shows the sputtering chamber used in this study. There are three guns that can be ignited at the same time. The cooling water pass through guns

and sample holder to cool them down. Stepper motor which is controlled with the software allows the sample holder rotates and stands at the top of each gun for certain amount of time.

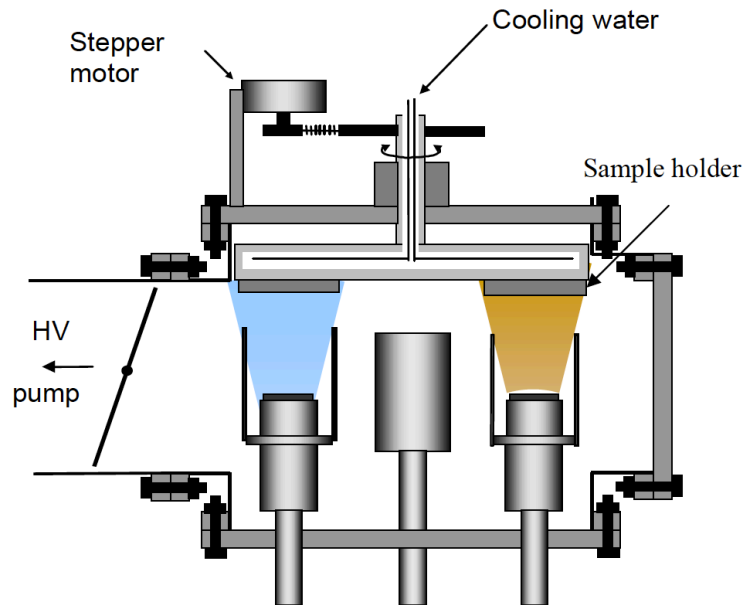


Figure 2.1: This schematic shows the sputtering chamber.¹¹

After placing targets and samples into the chamber, the chamber was pumped down and purged with nitrogen for couple of times, before opening the chamber to the high vacuum. To decrease water vapor and achieve higher vacuum, chamber was backed for 2 hours. High vacuum in the chamber can achieve to 8.8×10^{-7} Torr. High purity Argon gas with working pressure of 5 mTorr was used to sputter targets. Power

for CoPt target was 22watt and for silver was 11watt. The thickness of layers was controlled with the sputtering time.

To have CoPt and silver multilayers, the substrate swiping the guns at the specific time duration.

2.2 Heat Treatment

The as-deposited sample has the structure of fcc CoPt and fcc Ag. To get fct CoPt according to the phase diagram, it is crucial to do heat treatment on the sample.

The heat treatment was done by sealing the sample in the glass tube and placing it in the oven. The usual annealing temperature used was between 600°C and 750°C. During the heat treatment for sufficient time and at right temperature, CoPt nanoparticle with L1₀ phase are formed.

2.3 Sample Characterization

After preparing the sample, it is crucial to characterize the sample. For this purpose, different techniques were used.

2.3.1 X-ray Diffraction

X-ray diffraction(XRD) is to determine composition of the sample, phase and lattice constant, and degree of the ordering of L1₀ phase.

XRD Rigaku Ultima IV diffractometer was used to study samples. This diffractometer produces Cu K α radiation with wavelength 1.5406°A.

When x-ray radiations are incident on crystal lattice, some of them will be reflected from the surface of the crystal, while others penetrate through the crystal, and reflected from inner plane of crystals. When the difference of the path length of two reflected waves is equaled to integer number multiplied by x-ray wavelength, we have

constructive interfere, and Bragg's peak in the spectrum is seen. This concept is expressed by Bragg's law:

$$2d\sin\theta = n\lambda \quad (2.1)$$

In this formula, d is the spacing between lattice plane, $2d\sin\theta$ is path difference between two waves undergoing the interfere, λ is x-ray wavelength, n is integer number and θ is scattering angel (Figure 2.2).²² Since each lattice has different d spacing, Bragg's peak for each lattice occurs at different angles.

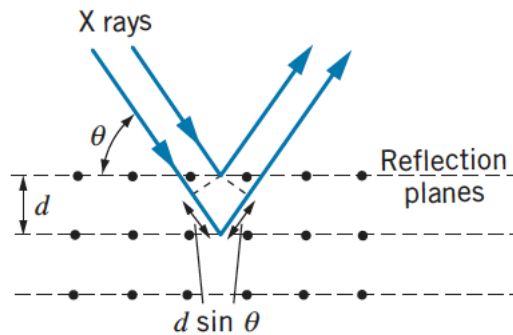


Figure 2.2: Bragg's diffraction from atoms of crystal. d is the distance between the crystal's plane.²²

Also, there is the selection rule that prohibit some of the peaks that the Bragg's law allows them to occur. For example, peaks allowed in fcc structure should have miller indices of all odd or even. While mixed miller indices of (hkl) can be observed in the ordered structure. Those peaks that emerged in only ordered structure are called superlattice peaks.²³

2.3.2 Vibrating Sample Magnetometer

Vibrating sample magnetometer (VSM) is used to measure magnetic properties of the sample.

A sample is placed between detecting coil and starts oscillating. Because of this oscillation, magnetic flux is changing, and it results in inducing voltage which is proportional with magnetic moment of a sample.

Quantum design verlab VSM was used to study the magnetic properties of samples.

2.3.3 Transmission Electron Microscopy

Transmission electron microscopy (TEM) used to study microstructure as well as structure of a sample. Jeol JEM-3010 Transmission Electron Microscope used to study this work.

From tungsten filament, electrons are emitted, hit the very thin specimen, and interact with it by elastic or inelastic collision. The image mode and the diffraction mode are two operation modes of Transmission electron microscopy. In image mode, a focused electron beam penetrates through a sample and form an image. There are two different imaging kinds: Bright field and dark field. In bright field, a central transmitted electron's beam is used and the image shows particles with all orientations. Dark field is obtained by diffracted electron's beams and shows particles with specific orientation.

Selected area diffraction (SAD) can be also obtained with TEM. SAD is very useful to determine the structure and phase of a sample.^{11,24}

Chapter 3

RESULTS AND DISCUSSIONS

3.1 CoPt Thin Film

The focus of this section is on the single CoPt thin film with thickness 100 nm. The XRD pattern of the as-deposited sample shows the clear disordered fcc structure with the broad (111) Bragg's peak at 40.5 degrees. This broad peak looks like an amorphous structure and shows that the as-deposited sample consists of very fine particles. Also (200) Bragg's peak is very broad and overlapped with (111) CoPt peak. One important information that can be obtained from any XRD pattern is the lattice parameters. Therefore, by using the XRD pattern of the as-deposited CoPt, we can find the lattice parameter of disordered fcc structure. Comparing this lattice parameter with the Figure 1.9 gives us the composition of the CoPt sample. Because (111) peak is very broad for this as-deposited sample, this method cannot be used. To solve this problem, the as-deposited CoPt was annealed at 900°C for 30 min. Since 900°C is much higher than CoPt ordering temperature, no transformation from fcc to fct can happen. The XRD pattern of annealed sample at 900°C shows very sharp and intense peak along (111) direction. This sharp peak shows the appearance of the large single crystal particle instead of very fine particles. Also, very short peak along (200) emerged after annealing at 900°C. The lattice parameter obtained from this pattern is $a=3.768\text{\AA}$. Based on Figure 1.9, the atomic composition of the CoPt is 54 percent Cobalt and 46 percent Platinum which is very close to equiatomic composition.

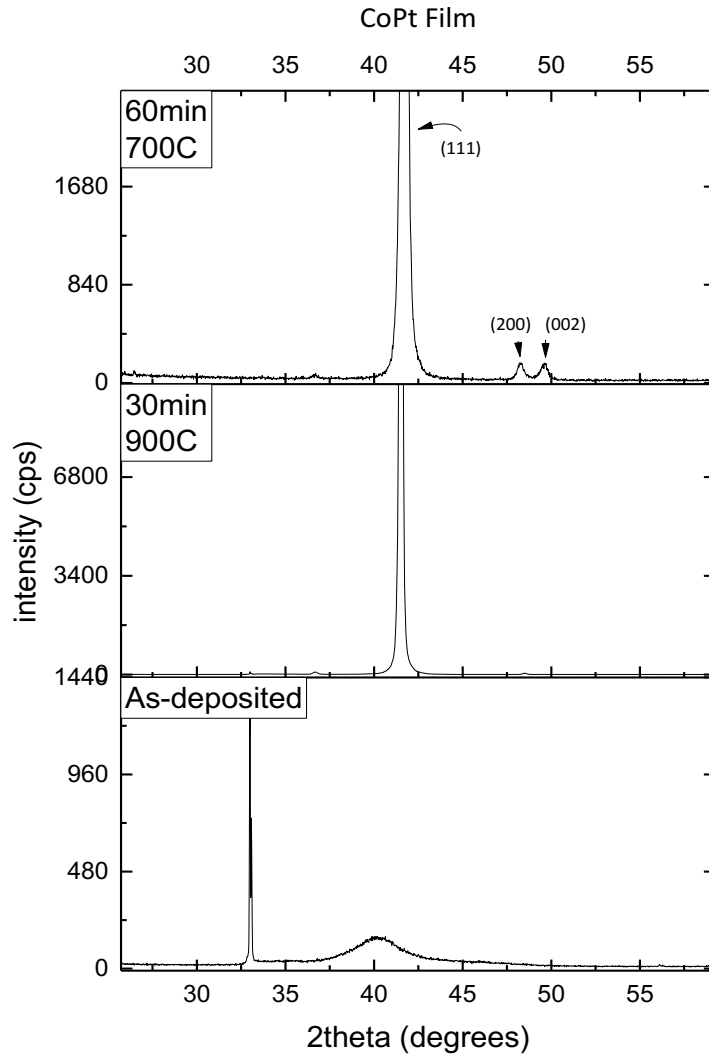


Figure 3.1: The XRD pattern of as-deposited, annealed at 900°C, and 700°C CoPt single film. The sharp peak around 33 degrees is from the Si substrate.

To obtain the $L1_0$ structure, the CoPt single film was annealed at 700°C for 60 min. The XRD pattern shows emergence of superlattice peak, (001), and the splitting of (200) and (002) peaks which suggest the transformation from disordered fcc to $L1_0$ phase. The lattice parameter of this $L1_0$ is $a = 3.767\text{\AA}$, $c = 3.668\text{\AA}$, $c/a = 0.9736$.

In this pattern, the (111) peak is much more intense than (001) peak, and it suggests a single crystal along (111) direction.

Also, the hysteresis loop for the as-deposited film shows very low coercivity (figure 3.2). This low coercivity suggests that the as-deposited CoPt film is a soft ferromagnetic material because the cubic structure has a low anisotropy. This low H_c supports the XRD conclusion that the as-deposited film has the disordered fcc structure. Annealed film at 700°C shows very high coercivity, 9.2 kOe, that originates from its high anisotropy energy due to the fct structure.

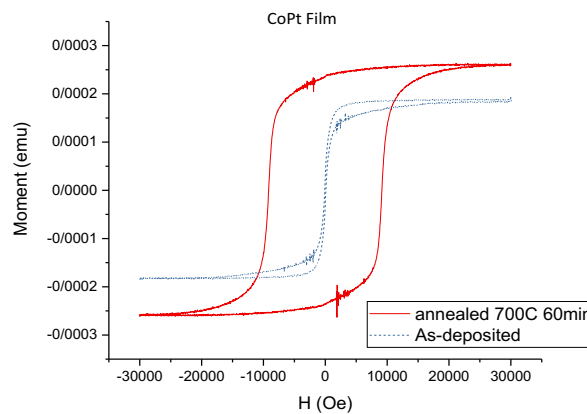


Figure 3.2: The hysteresis loops for as-deposited and annealed CoPt thin film. The as-deposited CoPt thin film shows very low coercivity, while the annealed CoPt thin film shows very high coercivity.

3.2 As-deposited and Annealed CoPt/Ag

The multilayer technique is used to fabricate the CoPt nanoparticles with $L1_0$ structure. In this study, the thickness of CoPt layer and total thickness of the samples were kept the same, and the effect of silver layer thickness was studied. CoPt layer has

a thickness of 5 nm, and silver layer has different thickness varying from 0.6nm, 2nm, 5nm, and 10nm. The samples were prepared all with the same condition, the same sputtering power, high vacuum pressure, Argon flow and pressure, substrate temperature, and post annealing conditions.

3.2.1 Structural Properties of the As-deposited and Annealed CoPt/Ag

The XRD pattern of all the as-deposited and annealed samples are shown in the figure 3.3.

Because of the absence of superlattice peaks and the splitting of (200) and (002) peaks in the XRD patterns of all as-deposited CoPt/Ag multilayer films, we can conclude that the as-deposited CoPt/Ag films have the disordered fcc structure like as-deposited CoPt single film. Low coercivity of these multilayers is also another indication of the disordered fcc structure. The satellite peaks around the Bragg's peak indicates a high degree of roughness in the multilayer structure of the as-deposited film.⁹

After annealing at 700°C, the superlattice peaks emerged and the (200) peak separated to the (200) and (002) peaks which indicate the presence of the $L1_0$ structure. The peaks at 38° and 44° are (111) and (200) silver.

Integrated intensities ratio of $I_{(001)}/I_{(111)}$ indicates the degree of (001) orientation of a sample.¹² Comparing this ratio for the CoPt single film and the CoPt/Ag shows that this ratio is higher for the samples with larger Ag layer thickness (Figure 3.4).

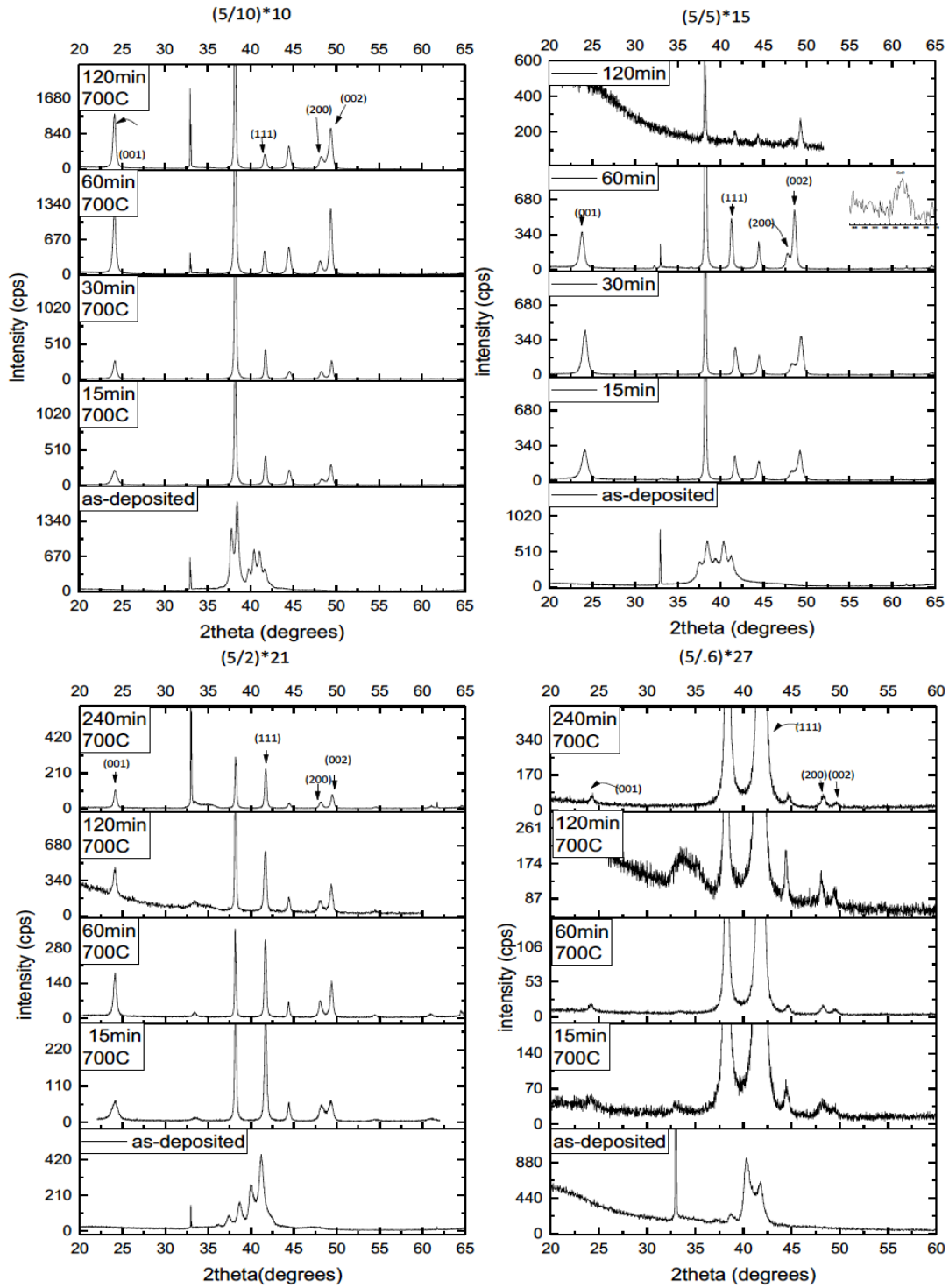


Figure 3.3: XRD patterns of the [(CoPt)5nm/(Ag)t]n multilayer samples. The peak at 33° is from substrate. Silver has peaks at 38° and 44°.

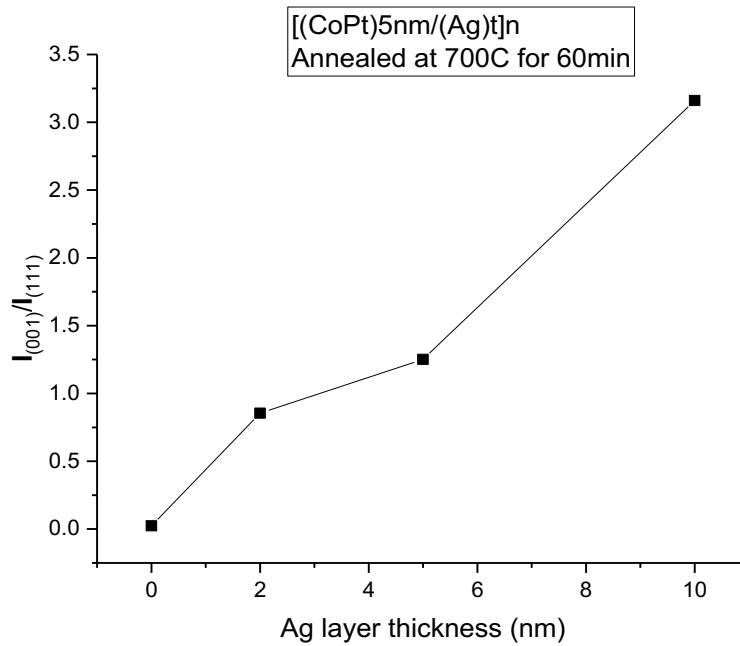


Figure 3.4: This figure shows the integrated intensities ratio of $I_{(001)}/I_{(111)}$ for annealed $[(\text{CoPt})5\text{nm}/(\text{Ag})t]_n$ sample with $t=0, 2, 5$ and 10 nm. Annealing was done at 700°C for 60 min.

3.2.2 Magnetic Properties of As-deposited and Annealed CoPt/Ag

3.2.2.1 Hysteresis Loop of CoPt/Ag

Figure 3.5 shows the hysteresis loops for all CoPt/Ag with different layer thickness for silver. Here, the as-deposited CoPt/Ag sample is a soft magnetic material with very low coercivity. The annealed CoPt/Ag sample is a hard magnet with very high coercivity.

The shoulder that appears in the hysteresis loops for the annealed $(5/5)$ nm*15 samples, the annealed $(5/10)$ nm*10 for 120min and the annealed $(5/.6)$ nm*26 for 15

min suggests the presence of two different soft and hard phases. Soft phase is attributed to fcc CoPt.

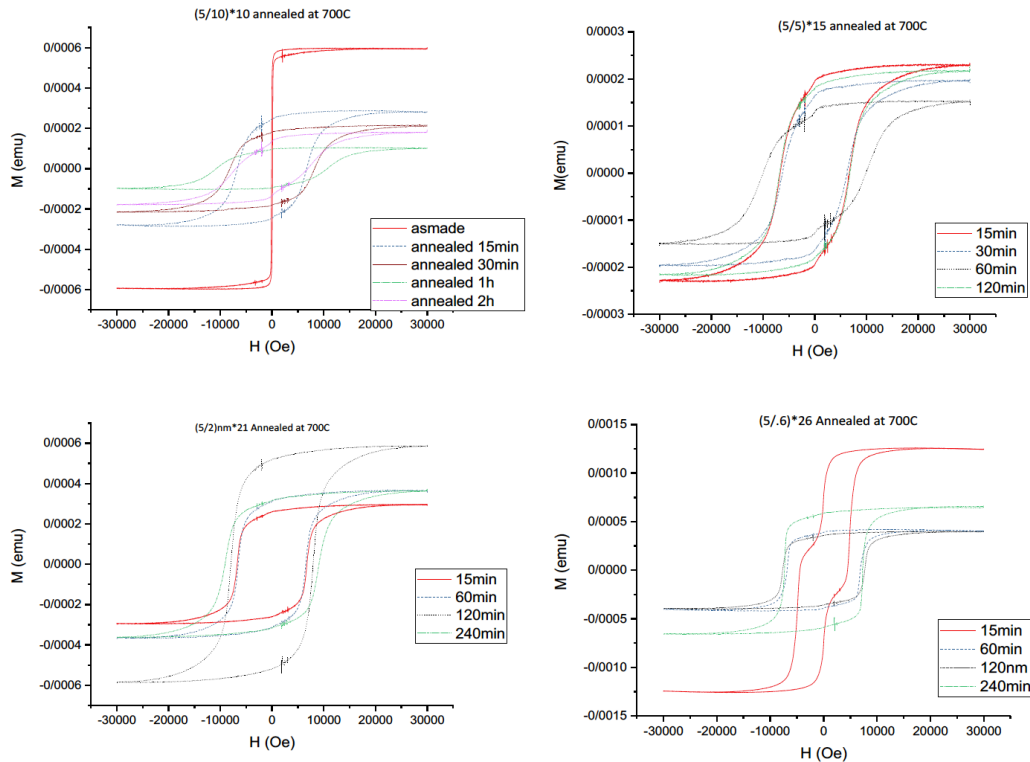


Figure 3.5: This figure shows the hysteresis loops for the as-deposited and the annealed [(CoPt)5nm/(Ag)t]n samples with $t=0.6, 2, 5$ and 10 nm .

3.2.2.2 Dependence of Coercivity on Annealing Time

The below figure shows the coercivity versus annealing time for (5/10) nm*10, (5/5) nm 15, (5/2) nm* 21 and (5/.6) nm* 26, annealed at 700°C. This graph suggests that for samples with thickness of Ag layer of 10nm and 5nm, the coercivity increases with annealing time, reaches its maximum value, and then decreases. Coercivity

depends on the particle size, the degree of ordering, and the interaction between particles, with the first two as the main contributions. The defects and impurities are other factors that can affect coercivity.

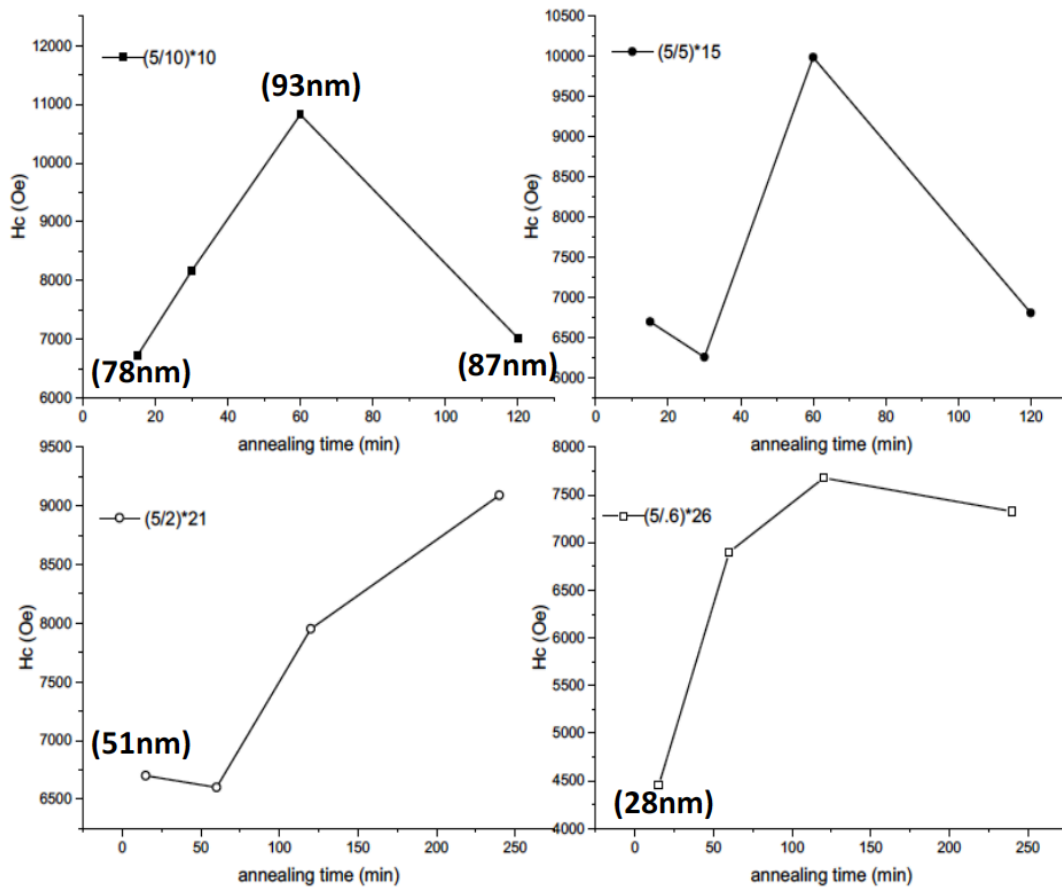


Figure 3.6: Coercivity versus annealing time. Annealing was done at 700°C.

TEM results from $(5/10)$ nm*10 sample suggests that the particle size increases by annealing time, and has its maximum value after 60 min annealing, and decreased after 120 min annealing. While the trend in the particle size agrees with the trend in

the coercivity, it cannot be the only factor to be responsible for this change in coercivity.

Figure 3.7 shows the c/a versus annealing time. A fully ordered sample has the minimum possible value for c/a .¹⁵ Also, the more ordered the sample is the higher the magnetocrystalline anisotropy which results in higher coercivity. Figure 3.7 shows the c/a for the (5/10) nm*10 sample is minimum after 30min and 60min annealing, and its value increased after 120 min annealing. The increase of the c/a after 120min annealing can be explained by the formation of the fcc CoPt phase. The shoulder in the hysteresis loop of this sample suggests the presence of the soft phase along with the hard phase. Because the XRD peaks of the fcc phase overlaps with $L1_0$ CoPt, it is hard to observe them in the XRD or the SAD patterns. It is also worth to mention that these coercivities were measured by applying the in-plane field. The integrated intensities ratio of $I_{(001)}/I_{(111)}$ which indicates the degree of (001) orientation was found for the (5/10)*10 samples annealed for 60 min and 120 min to be 3.2 and 4, respectively. Based on these values, if we apply the out-plane magnetic field, measured coercivity will increase for both samples annealed for 60 min and 120 min. Since the $I_{(001)}/I_{(111)}$ ratio is larger for the sample annealed for 120 min, the increase in the coercivity will be larger than the one annealed for 60 min. In other words, the difference between these two values of coercivity will be decreased, if the out-plane field is applied.

For the (5/5) nm*15 sample, the c/a is minimum after 30 min annealing, and it increased after 60 min annealing. This increase in the c/a after 60 min annealing can be explained by oxidization of cobalt during annealing. The XRD pattern of this sample shows a small peak of CoO. CoO results in less ordering in the sample, also it

can act as an impurity and results in higher coercivity due to pinning of the domain's walls. The presence of the shoulder in all the hysteresis loops of this sample suggest the existence of soft and hard phase, and it can explain why the (5/5) nm* 15 sample is less order in comparison with (5/10) nm*10.

For the (5/2) nm*21 and (5/.6) nm*26 samples, figures 3.6 and 3.7 shows the increase of the coercivity by annealing time due to the decrease of the c/a by annealing time.

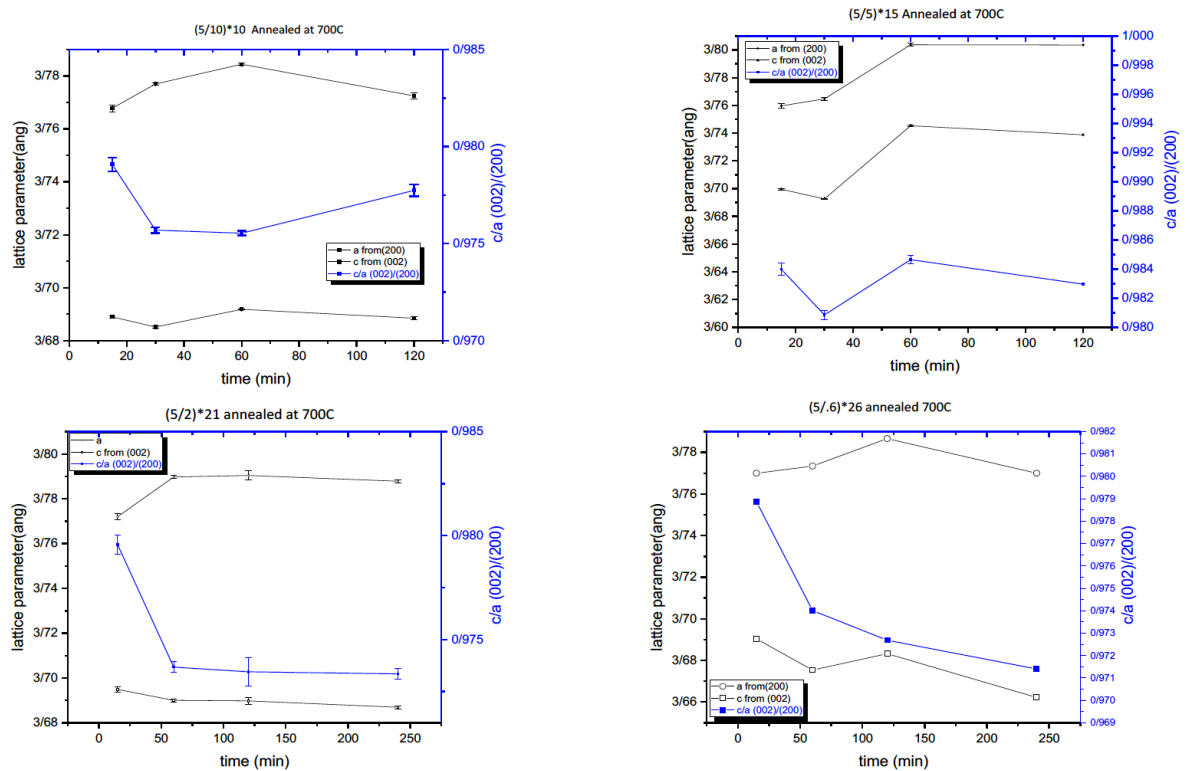


Figure 3.7: This figure shows the lattice parameters and the c/a for the samples annealed at 700°C. a and c were found from d spacing of (200) and (002) peaks, respectively.

Also, the figure 3.7 suggests that the samples with lower silver layer thickness is more ordered in comparison with the ones with larger silver layer thickness. The lowest value for c/a belongs to (5/.6) nm *26 after 240 min annealing.

The figure 3.8 compares the coercivity with silver layer thickness for two different annealing times. This figure suggests that the larger silver layer thickness results in higher coercivity at shorter annealing time. Also, the highest value for coercivity belongs to the sample with higher silver layer thickness which can be because of larger CoPt nanoparticles size.

In summary, the trend for the coercivity observed in the Figure 3.6 can be explained by the trend of the c/a . Based on the figures 3.6 and 3.7, for each sample, H_c increased, When the c/a decreased. It is because the coercivity is proportional to the magnetocrystalline anisotropy, and the magnetocrystalline anisotropy is larger when the c/a is smaller. The only exception was the annealed (5/5) nm*15 sample for 60 min. In this sample H_c is maximum after 60 min annealing, while its c/a is also maximum. This behavior can be explained by the formation of CoO. CoO acts as an impurity and increases the coercivity, while it decreases the degree of ordering. Also, because Ag makes diffusion harder, the samples with smaller Ag layer thickness are more ordered. Although the samples with smaller Ag layer thickness are more ordered, they have lower coercivity in comparison with the samples with larger Ag layer thickness. It can be because of the larger particle size of the samples with larger Ag layer thickness. Moreover, larger Ag layer thickness results in higher coercivity at shorter annealing time.

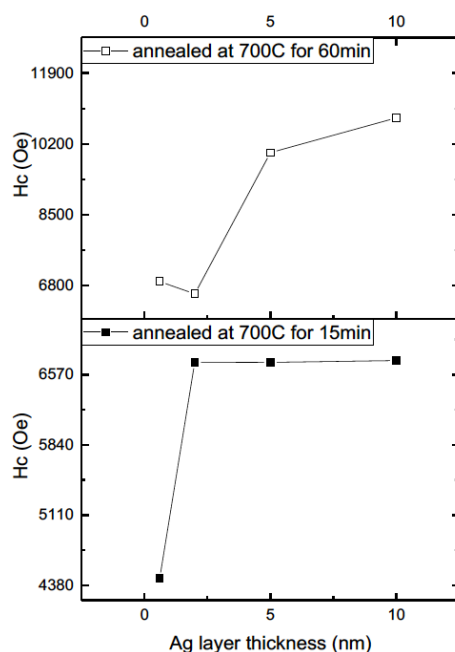


Figure 3.8: This figure compares the coercivity with the silver layer thickness for two different annealing times.

3.2.2.3 Coercivity as a Function of Temperature

The value for coercivity depends on temperature. Figure 3.9 shows the hysteresis loops for the (5/10) nm*10 sample annealed for 1h at 700°C. These loops show the coercivity is lower at higher temperature. Temperature dependence of coercivity is used in the high density recording to write on the media with high coercivity.³

In the presence of an external field, magnetization reversal energy barrier is given by equation 3.1, where H_0 is the intrinsic switching field. In the absence of an external field, E_B is K_uV , and its value is zero, when $H=H_0$. Therefore, increasing field from zero to H_0 results in reduction of the energy barrier.

$$E_B(H, V) = K_u(T)V \left(1 - \frac{H}{H_0}\right)^{1.5} \quad (3.1)$$

In this equation K_u depends on temperature, and its value decreased by increasing temperature. Therefore, energy barrier becomes smaller when temperature increases. For finite temperature, E_B should be compared with the thermal activation energy, $k_B T$.³ Magnetization will be reversed, when $k_B T$ is enough to overcome this energy barrier. When temperature is increased, the thermal activation energy is also increased. Therefore, $k_B T$ can overcome larger energy barrier. Also, based on the equation 3.1, the magnitude of the energy barrier depends on the magnitude of an applied field and temperature. Therefore, increasing temperature results in the thermal activation energy overcomes the smaller energy barrier at a lower applied field. In other words, increasing temperature results in lowering the coercivity.

Figure 3.10 shows the coercivity as a function of temperature which shows linear behavior.

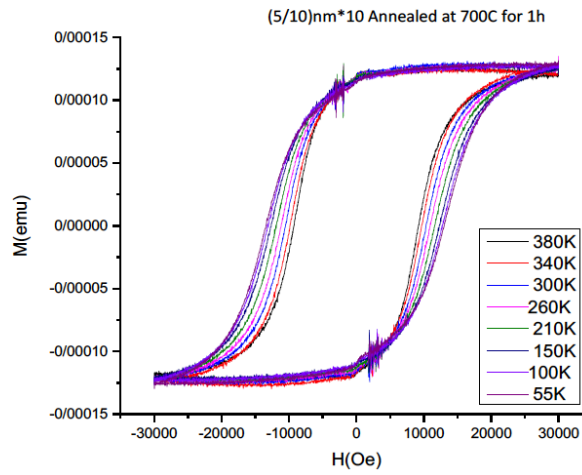


Figure 3.9: This figure shows the hysteresis loops for the (5/10) nm*10 sample annealed for 1h at 700°C. Coercivity increased when measurement done in lower temperature.

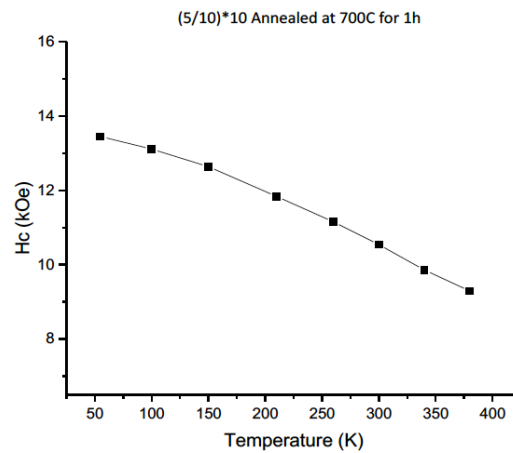


Figure 3.10: Coercivity as a function of temperature for the (5/10) nm*10 sample annealed at 700C for 1h.

3.2.3 Annealing Temperature Effects on the Structure and the Magnetic Properties of CoPt/Ag

The figure 3.11 shows the XRD pattern for the (5/10) nm*10 and (5/2) nm*21 samples annealed at 600°C, 700°C and 750°C for 60 min. The XRD patterns of the samples annealed at 700°C and 750°C show the same behavior. For the (5/10) nm*10 annealed at 600°C, (002) and (200) peaks are not completely separated from each other, and more time is required for this sample to become ordered. For the (5/2) nm*21 sample annealed at 600°C for 60 min, (200) disordered fcc peak broadened to become (200) and (002) peaks, while (001) superlattice peak is just emerging.

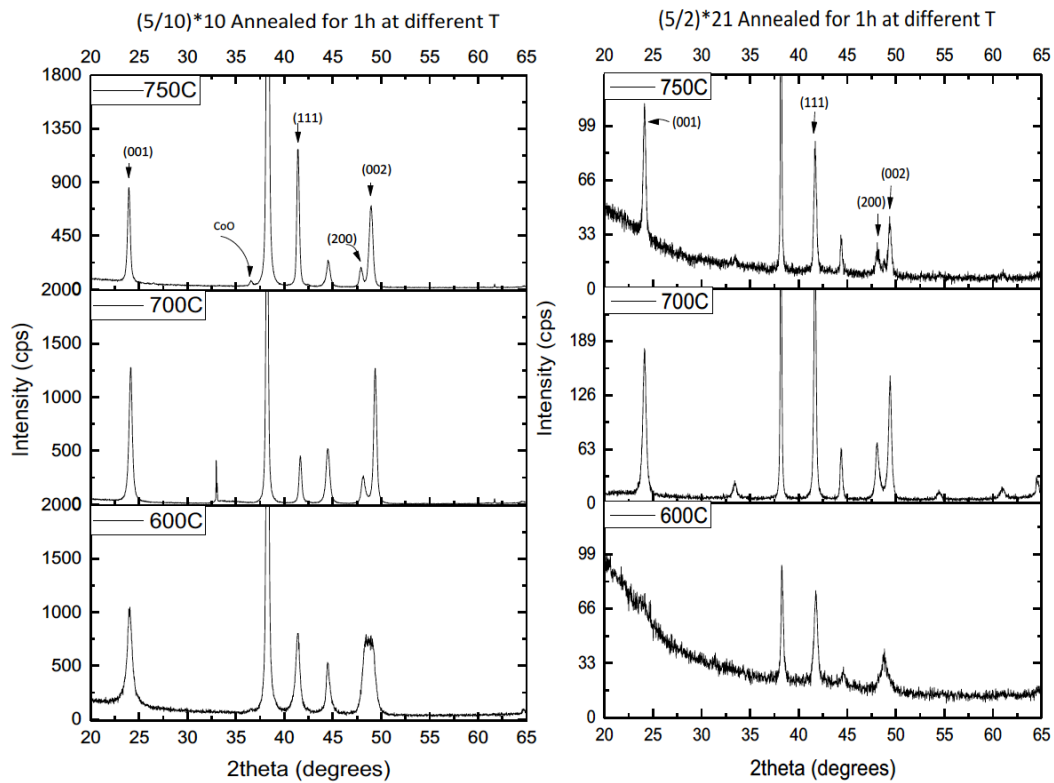


Figure 3.11: XRD patterns for the (5/10) nm and (5/2) nm samples annealed at 600°C, 700°C and 750°C for 60 min.

The figure 3.11 suggests that the sample with smaller silver layer thickness needs higher temperature or more annealing time to become ordered. It suggests larger layer thickness for silver in the CoPt/Ag can lower the activation energy required for CoPt to do transformation from the fcc to the fct structure. Previous studies found that adding silver in CoPt reduces the activation energy and increase degree of ordering¹². However, when the temperature is high enough for the (5/2) nm sample to order, its degree of ordering is higher in comparison with the (5/10) nm sample. It is because more silver makes diffusion harder, and decrease the degree of ordering.

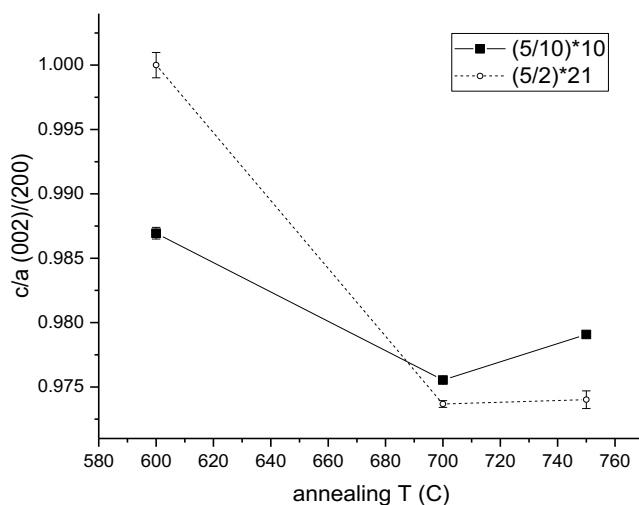


Figure 3.12: This figure shows c/a found from (002) and (200) peaks for (5/10) nm*10 and (5/2) nm*21 samples annealed for 60 min at three different temperature.

The figure 3.12 also shows there is no significant change in the degree of ordering of the (5/2) nm*21 sample annealed at 700°C and 750°C. However, the

(5/10) nm*10 sample annealed at 750°C is less ordered than the one annealed at 700°C. CoO peak was observed in the XRD pattern of this sample and it can be the reason for lower degree of ordering of this sample compared with the one annealed at 700°C. The presence of CoO can change the composition and result in the formation of the fcc phase. The shoulder in the sample's hysteresis loop shows the presence of the fcc structure. The presence of CoO can also explain high coercivity of this sample, since CoO can act as an impurity by pinning the domain walls.

The figures 3.13 and 3.14 show the hysteresis loops and coercivity versus annealing temperature. For the (5/2) nm*21 sample, H_c increased significantly by the annealing temperature from 600°C to 700°C. This increase can be explained by the increasing of the degree of ordering of the sample. While the degree of ordering did not change by annealing at 750°C, the coercivity decreased. It can be because of the particles with the sizes below and above the single domain particle size. The shoulder in the hysteresis loop of this sample supports this possibility.⁹ The (5/10) nm*10 sample annealed at 700°C has higher H_c in comparison with the one annealed at 600°C which is because of the higher degree of ordering. The presence of CoO in the annealed (5/10) nm*10 at 750°C results in lowering the degree of ordering and increasing the coercivity.

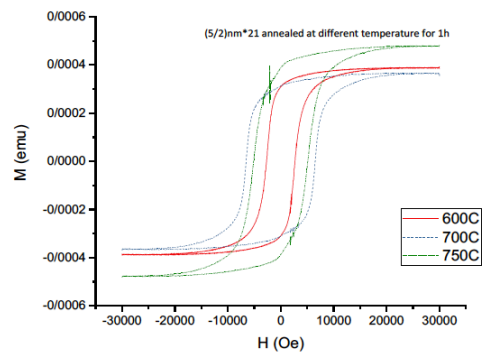
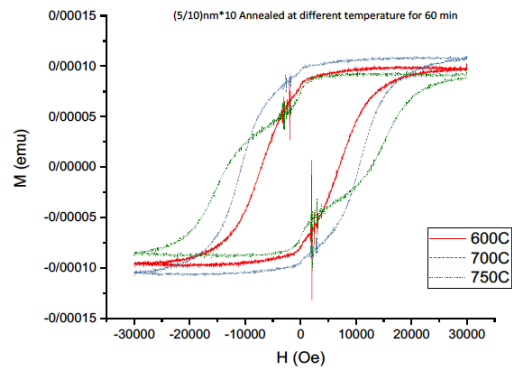


Figure 3.13: Hysteresis loops for (5/10) *10 and (5/2) *21 samples annealed for 60min at different temperatures.

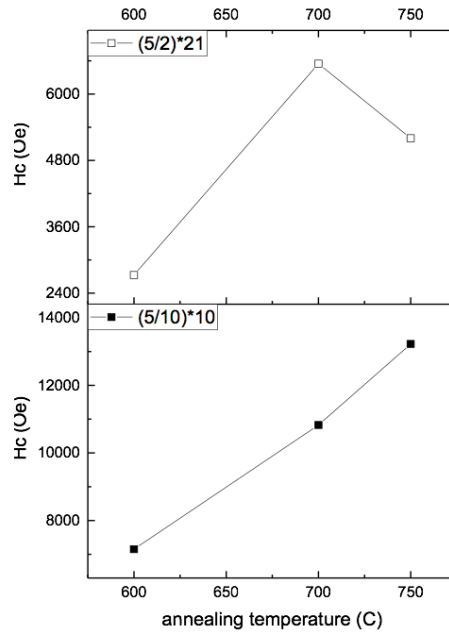


Figure 3.14: H_c versus annealing temperature.

3.2.4 Microstructure of As-deposited and Annealed CoPt/Ag

The below figure shows the microstructural of the as-deposited CoPt/Ag sample and the annealed CoPt/Ag samples. The as-deposited CoPt/Ag sample shows the uniform structure with very small particles. The same behavior was observed in its XRD pattern. Also, the selected area diffraction pattern (SAD) shows the fcc structure for CoPt and silver. No presence of the superlattice peaks or the splitting of (200) and (002) peaks are observed in the as-deposited CoPt/Ag. This result confirms the results from the XRD pattern and H vs M graph that as-deposited CoPt/Ag has the fcc structure.

After annealing, the $L1_0$ nanoparticles with larger size were developed. The SAD patterns show the presence of the fct structure. The TEM studies for most of the samples show that increasing silver layer thickness results in larger nanoparticles.

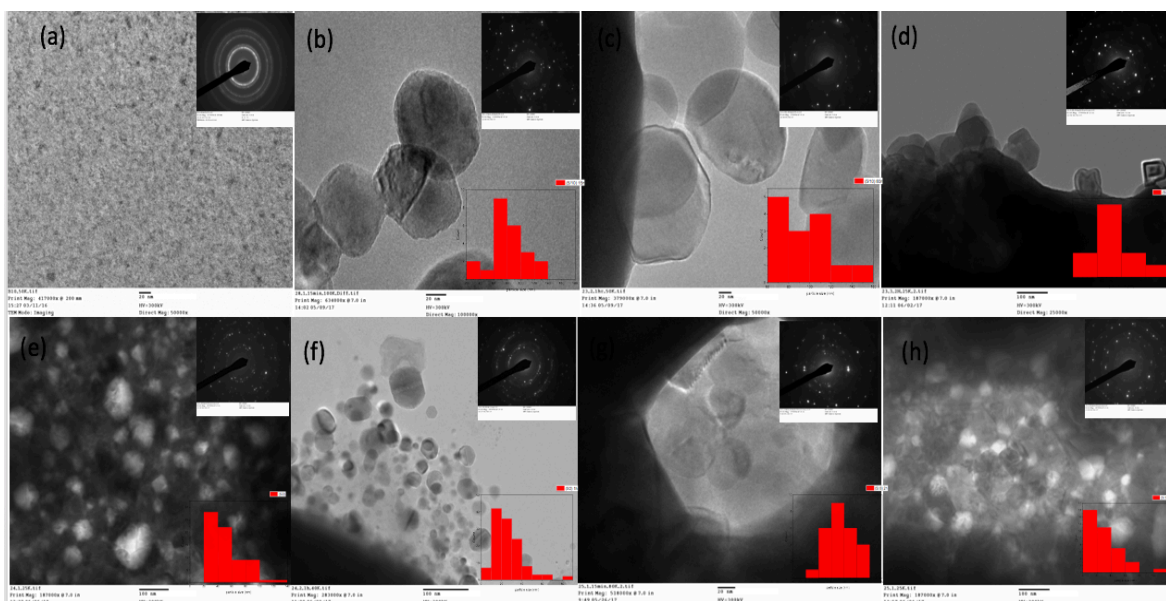


Figure 3.15: (a) As-deposited (5/2) nm. SAD pattern shows fcc structure for CoPt and Ag. (b) (5/10) nm annealed at 700°C for 15min. The average particle size is 79.7nm \pm 25nm. (c) (5/10) nm annealed at 700°C for 60min with average particle size of 93nm \pm 23nm. (d) (5/10) nm annealed at 700°C for 120min. The average particle size is 87nm \pm 42nm. (e) (5/2) nm annealed at 700°C for 15min with average particle size of 51nm \pm 22nm. (f) (5/2) nm annealed at 700°C for 60min with average particle size of 26nm \pm 14nm. (g) (5/.6) nm annealed at 700°C for 15min with average particle size of 28nm \pm 22nm. (h) (5/.6) nm annealed at 700°C for 120min with average particle size of 27nm \pm 11nm.

Chapter 4

CONCLUSION

The structural and magnetic properties of the as-deposited and annealed CoPt/Ag were studied in this thesis. L1₀ CoPt nanoparticles embedded in silver can be a potential candidate for high density recording media. Due to their tetragonal structure, L1₀ nanoparticles have very high magnetocrystalline energy that makes these particles thermally more stable.

The effect of silver layer thickness on the structure, degree of ordering, magnetic properties and particle size were investigated. For this, different CoPt/Ag multilayer samples were prepared with the same CoPt layer thickness, and different Ag layer thickness. Magnetron sputtering was used to fabricate the multilayers. XRD and SAD patterns and hysteresis loops for all as-deposited CoPt/Ag show that they have the fcc structure and are magnetically soft. The same behavior was observed in the CoPt single thin film.

Heat treatment is required for the Co and Pt atoms to diffuse and form the ordered L1₀ structure. CoPt/Ag annealed at 700°C shows very high coercivity and their XRD and SAD patterns show the L1₀ phase. It has been found that samples with larger Ag layer thickness can have larger coercivity, and their ordering is achieved at lower temperature and shorter annealing time in comparison with the ones with smaller layer thickness for silver. However, samples with lower Ag thickness are more ordered than the ones with larger Ag thickness. Also, the effect of annealing temperature was investigated here. The (5/2) nm*21 and (5/10) nm*10 samples annealed at three different temperatures for 60 min. The results show that annealing at 600°C for 60 min is not enough to order the samples, and longer annealing time is

required. Also, (5/10) nm sample annealed at 600°C is more ordered than (5/2) nm sample annealed at 600°C. This confirms the result of previous section that ordering for samples with larger Ag thickness happens at lower temperature and shorter time. This indicates that Ag lowers the activation energy required to transform the fcc to fct phase. The (5/2) nm sample annealed at 700°C and 750°C for 60 min shows higher degree of ordering in comparison with the (5/10) nm sample annealed at the same temperature and time. Again, it confirms that for high enough temperature and annealing time, the sample with less silver is more ordered than the one with larger Ag. TEM results show that increasing silver layer thickness results in larger nanoparticles. This result can be the reason for higher coercivity in samples with larger Ag layer thickness.

For future works, to increase an areal density in the high density recording media, the size of the particles should be decreased. Therefore, it is important to fabricate L1₀ CoPt nanoparticles with smaller size. To do this, Ag layer thickness should be decreased. However, higher Ag layer thickness helps to lowering the activation energy required for the transformation from the fcc phase to the fct phase. Therefore, it is better to not only decrease the Ag layer thickness, but also decrease CoPt layer thickness. Also, using two different matrixes like C/Cu and Ag can be interesting.

REFERENCES

- 1 Krishnan, K. M. *Fundamentals and applications of magnetic materials*
- 2 Lu, A. H., Salabas, E. e. L. & Schüth, F. Magnetic nanoparticles: synthesis, protection, functionalization, and application. *Angewandte Chemie International Edition* **46**, 1222-1244 (2007).
- 3 Moser, A. *et al.* Magnetic recording: advancing into the future. *Journal of Physics D: Applied Physics* **35**, R157 (2002).
- 4 Weller, D. *et al.* High K/sub u/materials approach to 100 Gbits/in/sup 2. *IEEE Transactions on Magnetics* **36**, 10-15 (2000).
- 5 Laughlin, D. E., Srinivasan, K., Tanase, M. & Wang, L. Crystallographic aspects of L1 0 magnetic materials. *Scripta Materialia* **53**, 383-388 (2005).
- 6 Coey, J. M. D. *Magnetism and magnetic materials*.
- 7 Tannous, C. & Gieraltowski, J. The Stoner–Wohlfarth model of ferromagnetism. *European journal of physics* **29**, 475 (2008).
- 8 Morrish, A. H. *The physical principles of magnetism*
- 9 Stavroyiannis, S. *et al.* CoPt/Ag nanocomposites for high density recording media. *Applied physics letters* **73**, 3453-3455 (1998).
- 10 Panagiotopoulos, I., Stavroyiannis, S., Niarchos, D., Christodoulides, J. & Hadjipanayis, G. Granular CoPt/C films for high-density recording media. *Journal of Applied Physics* **87**, 4358-4361 (2000).
- 11 Wan, J. *FePt GRA ULAR FILMS FOR ULTRA-HIGH DE SITY RECORDI G*, (Winter 2009).
- 12 Chen, C., Kitakami, O., Okamoto, S. & Shimada, Y. Ordering and orientation of CoPt/SiO 2 granular films with additive Ag. *Applied Physics Letters* **76**, 3218-3220 (2000).
- 13 Ristau, R., Barmak, K., Lewis, L., Coffey, K. & Howard, J. On the relationship of high coercivity and L1 0 ordered phase in CoPt and FePt thin films. *Journal of applied physics* **86**, 4527-4533 (1999).
- 14 Hadjipanayis, G. C. *An investigation of magnetic hardening in platinum-cobalt and platinum-nickel-iron alloys*. (1979).
- 15 Khajehnezhad, A. & Sebt, S. Order Parameter in L10 FePt Nanocrystals. *Transactions of the Indian Institute of Metals* **67**, 903-907 (2014).
- 16 Yu, M., Liu, Y., Moser, A., Weller, D. & Sellmyer, D. J. Nanocomposite CoPt: C films for extremely high-density recording. *Applied Physics Letters* **75**, 3992-3994 (1999).

- 17 McCurrie, R. & Gaunt, P. The magnetic properties of platinum cobalt near the equiatomic composition part I. the experimental data. *Philosophical Magazine* **13**, 567-577 (1966).
- 18 Delaunay, J.-J., Hayashi, T., Tomita, M., Hirono, S. & Umemura, S. CoPt–C nanogranular magnetic thin films. *Applied physics letters* **71**, 3427-3429 (1997).
- 19 Charap, S. H., Lu, P.-L. & He, Y. Thermal stability of recorded information at high densities. *IEEE Transactions on Magnetics* **33**, 978-983 (1997).
- 20 Christodoulides, J. *et al.* Magnetic, structural and microstructural properties of FePt/M (M= C, BN) granular films. *IEEE transactions on magnetics* **37**, 1292-1294 (2001).
- 21 Swann, S. Magnetron sputtering. *Physics in technology* **19**, 67 (1988).
- 22 Krane, K. *Modern Physics*.
- 23 Hammond, C. *The Basics of Crystallography and Diffraction*. Fourth edn.
- 24 Reimer, L. *Transmission Electron Microscopy: Physics of Image Formation and Microanalysis*. (1984).